



Contents lists available at ScienceDirect

Engineering Science and Technology, an International Journal

journal homepage: www.elsevier.com/locate/jestch

Full Length Article

Adjacent surface trajectory planning of robot-assisted tooth preparation based on augmented reality

Jingang Jiang ^{a,b,*}, Yafeng Guo ^a, Zhiyuan Huang ^a, Yongde Zhang ^{a,b}, Dianhao Wu ^a, Yi Liu ^c^a Key Laboratory of Advanced Manufacturing and Intelligent Technology, Ministry of Education, Harbin University of Science and Technology, Harbin 150080, China^b Robotics & Its Engineering Research Center, Harbin University of Science and Technology, Harbin 150080, China^c Peking University School of Stomatology, Beijing 100081, China

ARTICLE INFO

Article history:

Received 3 January 2021

Revised 3 May 2021

Accepted 5 May 2021

Available online xxxx

Keywords:

Dental assisted robot

Adjacent surface tooth preparation

Trajectory planning

Augmented reality

NURBS curve

ABSTRACT

Dental caries is a common disease affecting the health of humans. Tooth preparation is an essential method for the treatment of dental caries, and its effect determines the quality of dental caries restoration directly. At present, the doctor-patient ratio of dentistry is incredibly unbalanced, and it is challenging to meet the increasing demand for tooth preparation. Besides, it is prone to produce visual deviation and positioning error if the tooth preparation is operated manually by doctors. This paper focuses on the adjacent surface tooth preparation of the full crown. By analyzing the preparation process, the robot body as well as the end-effector are selected. Further, the pose and position between the robot and the tooth are established. Through the inverse calculation and interpolation of the NURBS curve, the robot-assisted trajectory planning of adjacent surface tooth preparation is realized. On the basis of the traditional offline programming method, mobile App "Dental Preparation Assisting Software" is developed based on augmented reality, which can interactively display the planned adjacent preparation curves and preparation information. And the robot can be controlled by the mobile App, which improves the visualization and efficiency of the preparation process. Finally, the experimental system based on the Dobot Magician robot is established, and the robot experiments of adjacent surface tooth preparation are carried out. The maximum relative fixed-point error of each feature point in the XYZ axis is 0.24 mm, 0.29 mm and 0.37 mm, respectively. The confidence interval width of each feature point in the XYZ direction is stable at about 0.31 mm on average, and the correlation between the feature points in the three directional variables is not strong. The proposed method of robot-assisted trajectory planning based on augmented reality for adjacent surface tooth preparation can improve the efficiency of tooth preparation and relieve the pressure of manual tooth preparation within the margin of error, and its feasibility and validity are verified.

© 2021 Karabuk University. Publishing services by Elsevier B.V. This is an open access article under the CC BY-NC-ND license (<http://creativecommons.org/licenses/by-nc-nd/4.0/>).

1. Introduction

According to the World Health Organization, dental caries is a significant public health problem globally and the most widespread non-communicable disease (NCD). It is also the most prevalent condition included in the 2015 Global Burden of Disease Study, ranking first for the decay of permanent teeth (2.3 billion people) [1]. Dental caries is a common disease that affects the health of the population. It not only affects mastication, pronunciation, and appearance, but also has a very close relationship with systemic diseases such as stroke, coronary heart disease, diabetes, digestive system diseases, and respiratory system diseases. Tooth

preparation is a necessary part of the treatment of chipped and missing teeth. It requires the surgeon to manually remove the carious tooth quantitatively in the patient's mouth and form the desired tooth shape [2] for the subsequent placement of a metal or porcelain crown, which restores the morphology and function of the carious tooth in turn. The effectiveness of dental preparation directly determines the quality of the restoration of a carious tooth [3]. At present, the manual preparation of carious teeth requires several micro-adjustments in order to obtain the desired shape of the preparation due to the visual aberration of the human eye and manual positioning control errors, which is labour-intensive and inefficient [4]. In addition, there is a severe imbalance in the doctor-patient ratio in dentistry, which makes it challenging to meet the increasing demand for dental preparations [5].

* Corresponding author.

Peer review under responsibility of Karabuk University.

Augmented Reality (AR), is a technology that calculates the position and angle of camera images in real time and adds corresponding images, videos, and 3D models. The goal of this technology is to put the virtual world on the screen and interact with the real world. Due to the small size of teeth, the use of augmented reality technology can effectively improve the visualization of teeth and reduce preparation errors. In addition, the clinical dental preparation process is characterized by long operative time and repetitive operations, so the introduction of robotics into the field of dental preparation can relieve the pressure of manual preparation by replacing the doctor with repetitive preparation operations and improving the efficiency of dental preparation. Therefore, the application of augmented reality and robotics to dental caries dental preparation has become a hotspot of research in the field of medical robotics.

In terms of robotized dental preparation, Simon et al designed a dental-assisted robot for dentists to drill. The robotic system consisting of a robotic arm, force sensors and motor actuators, and a dental handpiece clamped at the end of the arm to perform dental drilling operations and complete in vitro testing [6]. Hang et al designed a robotic system for oral and dental treatment in which a physician controls a robotic arm in the patient's mouth through a console [7]. Kanuma et al designed an automated system for tooth preparation, and the robot performs anterior veneer extra-corporeal tooth preparation based on an existing tooth model and a model of a completed preparation [8]. Bello retrofitted a computerized numerical control machine and accessory device for in vitro full-crown tooth preparation [9]. Grischke et al outline the existing applications of robotic systems and artificial intelligence in dentistry [10]. Dai et al proposed a feature parameter-based tooth preparation modelling approach and developed a dental preparation design system to help dentists quickly personalize the morphological characteristics of prepared teeth [11]. Lyu and Yuan proposed the digital design of molar tooth preparation using Geomagic and Imageware, and developed an automated tooth preparation robot to control a high-power ultrashort pulsed laser beam to complete tooth preparation of isolated teeth in a mimetic head mold [12–14]. Wang et al developed a micro-robotized device, LaserBot, to drill decayed teeth using a picosecond laser for clinical crown preparation [15,16]. The above studies have made useful explorations of the application of robotics in dentistry, but none of them has investigated robot-assisted trajectory planning for tooth preparation.

Many researchers have combined augmented reality with robotics. Solymar et al propose an intuitive semi-automatic offline robot programming method based on Augmented Reality [17]. Huang et al. use augmented reality technology to provide a good remote control operating interface for human-robot interaction [18]. Zhang et al apply augmented reality in robot programming, which in turn improves the problem of offline programming of robots that requires providing a 3D model of the robot as well as its workspace [19]. Hernández et al give commands to the robot by designing the AR interface to go and can preview the robot's movements through augmented reality [20]. Chacko et al propose a novel augmented reality interaction method that allows robots to perform operations on unknown physical objects in a collaborative human-robot work environment. And the corresponding mobile software is designed [21]. The above studies have contributed favorably to the integration of robotics and augmented reality technology, but none of them have addressed the field of dental prosthetics.

To solve the problems mentioned above, the robot body as well as the end-effector will be selected, the positional relationship between the robot and the teeth will be established by analyzing the process of full crown adjacent surface tooth preparation in the posterior teeth. The trajectory of robot-assisted tooth prepara-

tion will be planned, then the software DPAS AR (Dental Preparation Assisting Software based on Augment Reality) will be developed. Compared to traditional offline programming, the doctors can rotate and zoom the planned preparation curve with DPAS AR to clearly display the planning details, and preview the results of adjacent surface preparation curve planning. These enhance the visualization and accuracy of the trajectory planning of the adjacent surface preparation. The software can display preparation information and control the robot to complete preparation operations, improving the human-robot interaction between the physician and the robot. Finally, experiments of robot-assisted adjacent surface tooth preparation will be carried out.

2. Methods

2.1. Process analysis of posterior full crown adjacent surface preparation

Posterior molars have a larger surface area and more grooves and sockets than anterior incisors and anterior cusps, so the caries rate in posterior teeth is significantly higher than in anterior teeth. Full crown preparation is preferred for posterior teeth, because it produces a preparation that is superior in retention and resistance to other types of preparation. The posterior full crown preparation process is divided into occlusal, adjacent surface and functional cusp bevel preparation. Adjacent surface preparation involves determining the shoulder width based on the width and shape of dental drill, performing buccal preparation, separating the adjacent teeth, and then achieving adjacent surface preparation. The procedure of full crown adjacent surface preparation of posterior teeth is shown in Fig. 1. The key to the operation of adjacent surface preparation is to control the width of the abutment while avoiding damage to the adjacent teeth and gums, as a narrow abutment will affect the precision, strength, aesthetics of the preparation and crown. At the same time, a wide abutment will damage too many healthy teeth or even the pulp, thus reducing the resistance of the tooth. Therefore, the analysis of robotic preparation of the adjacent surfaces will be focused in the article.

2.2. Establishment of a relationship between tooth preparation robots and dental posture

The Dobot Magician tandem articulated arm was selected as the robot body for the assisted tooth preparation robot. The dobot has 4 degrees of freedom and the robot has three rotational degrees of freedom for the small arm, the large arm and the base respectively. The end can withstand a load of 500 g, the maximum extension distance of the arm is 320 mm and the repeatable positioning accuracy is 0.2 mm, which meets the basic requirements of the dental preparation process. The tooth preparation robot is shown in Fig. 2.

2.2.1. The relationship between robot and tooth posture

Based on the robot model, the relationship between the robot and the tooth coordinate system is established. In addition to the base coordinate system {0} and end coordinate system {4}, the dental drill coordinate system {T}, tooth surface reference coordinate system {R} and target coordinate system of tooth preparation {G} are also introduced, each coordinate is shown in Fig. 3. Each coordinate is formed into a closed loop to obtain the actual relative position of the robot's tooth preparation for calculating the relationship between the coordinate dental drill system {T} and the tooth preparation target coordinate system {G}, as shown in Fig. 4.

Matrix relations are obtained through the upper and lower halves of the closed ring.

$$OT_G = OT_4 T_{TT} T_G \quad (3)$$

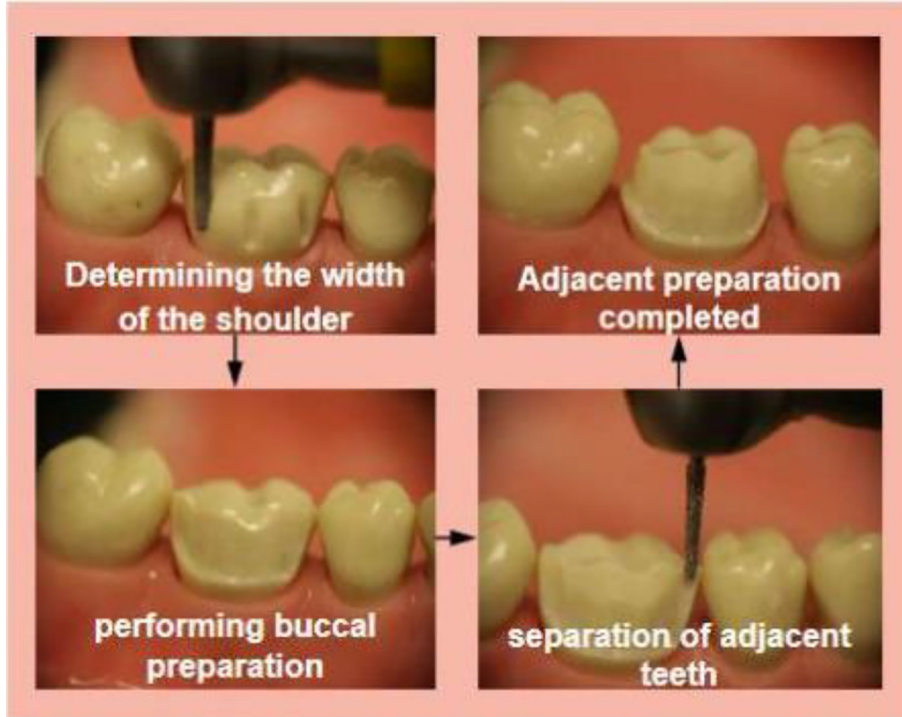


Fig. 1. Flow chart of the full crown adjacent surface preparation of the posterior teeth.

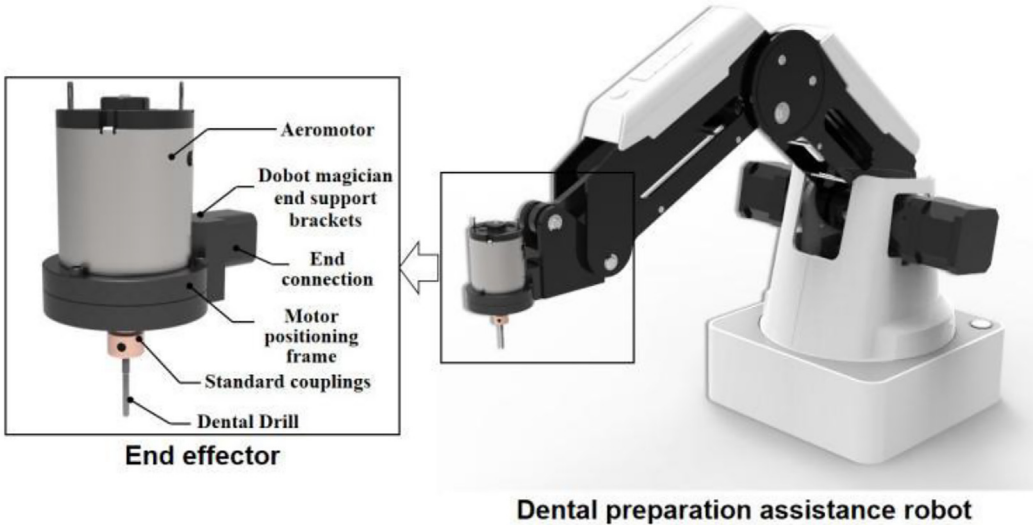


Fig. 2. Tooth preparation robot.

$$OT_G = OT_R RT_G \quad (4)$$

where OT_G is the positional matrix of the target coordinate system with respect to the robot base; OT_4 is the positional matrix of the robot end with respect to the robot base; $4T_T$ is the positional attitude of the dental drill with respect to the end; GT_T is the unit matrix; OT_R is the positional matrix of the reference coordinate system with respect to the robot base; and OT_R is the positional matrix of the target coordinate system with respect to the reference coordinate system.

Further, equation (5) is established by making equation (3) equals to equation (4).

$$OT_4 4T_T TT_G = OT_R RT_G \quad (5)$$

where, except for the OT_4 matrix, the rest are known matrices, so multiplying both sides by $4T_T^{-1}$ simultaneously gives the relative posture matrix of the robot's tooth reserve:

$$OT_4 = OT_R RT_G (GT_T^{-1}) (4T_T^{-1}) \quad (6)$$

The preliminary calculation of the coordinate transformation has been completed, and the following will be solved for the unknown matrix OT_4 , which is the kinematic positive solution calculation.

2.2.2. Analysis of forward kinematics

According to Dobot Magician under the joint coordinate system, parameters and relationships between each joint are defined in Fig. 5. The D-H method is used to establish the coordinate system

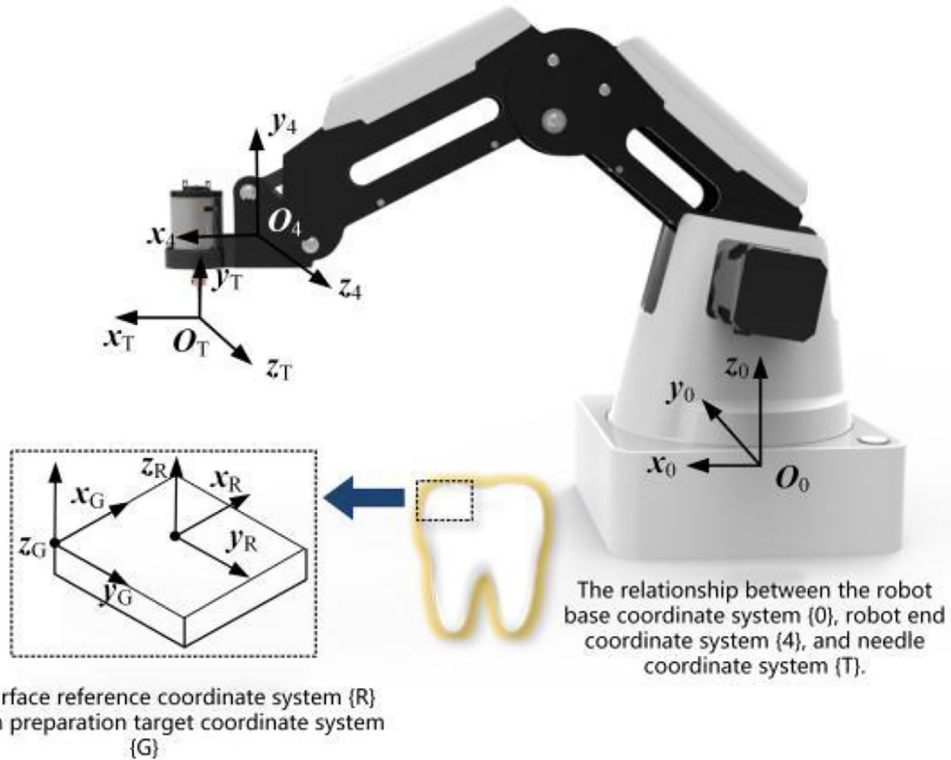


Fig. 3. The coordinate system in the robot.

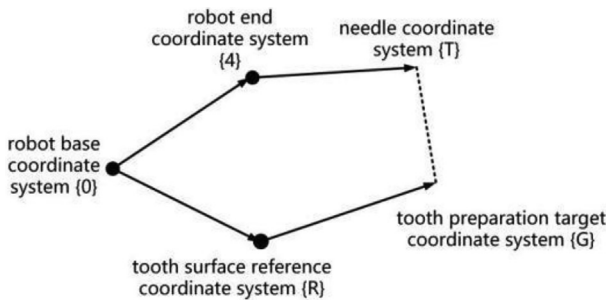


Fig. 4. A closed-loop for the coordinate system.

and axis orientation of each joint of the robot, as shown in Fig. 6. The D-H parameters of each joint of the robot are shown in Table 1.

Table: a_{i-1} is the metric perpendicular length of the joint axis, α_i is the angle between two adjacent coordinate system Z-axis, d_i is the joint variable for sliding joints, and θ_i is the joint variable for rotating joints.

The kinematic equation of the robot T is a concatenation of the transformation matrix of each coordinate system from the reference coordinate system of the base to the coordinate system of the robot's end, expressed as:

$$OT_N = OT_1 1T_2 2T_3 \cdots N - 1T_N \quad (7)$$

Positive kinematic equations for the tooth preparation robot are obtained by multiplying the congruent transformation matrix of the four joints.

$$OT_4 = OT_1 1T_2 2T_3 3T_4 \\ = \begin{bmatrix} R_{04} & P_{04} \\ 0 & 1 \end{bmatrix} = \begin{bmatrix} n_x & o_x & a_x & p_x \\ n_y & o_y & a_y & p_y \\ n_z & o_z & a_z & p_z \\ 0 & 0 & 0 & 1 \end{bmatrix} \quad (8)$$

where R_{04} denotes the pose, and P_{04} denotes the position.

$$n = \begin{bmatrix} s_1 s_2 (c_4(c_3 - s_3) - s_4(c_3 + c_3)) \\ s_1 (c_4(c_2 c_3 - s_2 s_3) - s_4(c_2 s_3 + s_3 c_3)) \\ c_4(s_2 c_3 + c_2 c_3) + s_4(c_2 c_3 - s_2 s_3) \\ 0 \end{bmatrix}$$

$$o = \begin{bmatrix} s_1 s_2 (-s_4(c_3 - s_3) - c_4(s_3 + c_3)) \\ c_1 (-s_4(c_2 c_3 - s_2 s_3) - c_4(c_2 c_3 + s_2 c_3)) \\ -s_4(s_2 c_3 + c_2 c_3) + c_4(c_2 c_3 - s_2 s_3) \\ 0 \end{bmatrix}$$

$$a = \begin{bmatrix} s_1 \\ -c_1 \\ 0 \\ 0 \end{bmatrix} p = \begin{bmatrix} s_1 s_2 (a_2(c_3 - s_3) + a_1) \\ s_1 (s_3 a_2(c_3 - s_2) + a_1 c_1) \\ (s_1 c_3 + c_2 c_3)a_2 + s_2 a_1 + d \\ 1 \end{bmatrix}$$

For convenience, the complex trigonometric functions in the above formula are replaced by abbreviations: s_1 represents $\sin\theta_1$, c_1 represents $\cos\theta_1$, s_2 represents $\sin\theta_2$, c_2 represents $\cos\theta_2$, and so on.

2.3. Adjacent surfaces trajectory planning for Robotic-assisted tooth preparation

The preprocessing process of the standardized posterior tooth prep model is shown in Fig. 7. Firstly, the standardized 3D model of a posterior tooth in 'obj' format is imported into Geomagic Wrap, a reverse engineering software, and then the model is prepped by using "grid doctor", "filling hole", "plane", and "mesh" in sequence. The commands such as "polished surface" and "tectonic surface sheet" are used to create a closed 3D model. Then the "structural grids" and "fitted surface" commands are used to connect multiple surface slices for generating surface and boundary features. And,

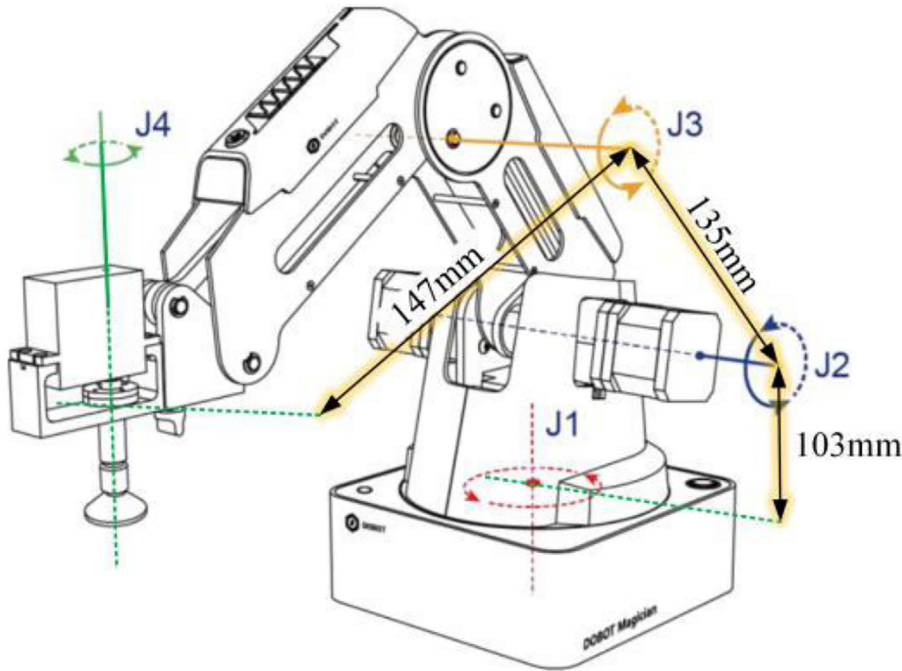


Fig. 5. Joint parameters and relationships of Dobot Magician.

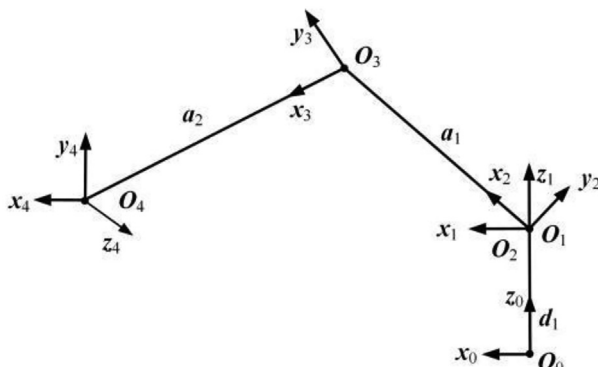


Fig. 6. Robot coordinate system.

subdivision meshes are constructed within each surface slice. Finally, the “fit surface” command is used to obtain a 3D model in ‘step’ format with surface and boundary features. In the standardized tooth preparation, 2/3 of the dental drill diameter D is inside the shoulder generated in the adjacent surface preparation stage. The remaining 1/3 D is outside the tooth, so the distance between the axis of the dental drill and the tooth edge curve C_L is 1/6 D , based on which the C_G of the robot’s adjacent surface preparation curve can be obtained, as shown in Fig. 8. The obtained 3D model in ‘step’ format was imported into Creo software, and the extraction, copying and offset of the tooth margin curve C_L of the standardized preparatory body was completed by the commands

“Copy” and “Offset” to obtain the standard adjacent surface tooth preparation curve C_G . A further standard adjacent surface tooth preparation curve C_G is used to obtain a plurality of discrete points Q for the next calculation of the curve by two parameters: the number of discrete points N_Q and the distance between the discrete points L_Q .

2.3.1. Introduction of NURBS curves and inverse calculation of tooth preparation curves on adjacent surfaces

Non-Uniform Rational B-Splines (NURBS), a common mathematical model for generating and representing curves and surfaces, provides great flexibility and accuracy to handle analytic models and modeled shapes [22]. Thus, the NURBS-based inverse calculation solves the adjacent surface tooth preparation curves. In the inverse calculation step, the parameters are known as discrete points Q and weight factor ω , and the inverse targets are node vector U and control point P . The NURBS-based inverse calculation step of the adjacent surface tooth preparation curve is as follows: a. Calculate the node vector U of the adjacent surface tooth preparation curve; b. Determine the boundary conditions at the beginning and end of the adjacent surface tooth preparation curve; c. Calculate the control point of the adjacent surface tooth preparation curve. First of all, the existing parametric method is selected to complete the calculation of the vector U of the nodes of the adjacent surface tooth preparation curve. As shown in Fig. 9, the uniform parametric method, cumulative chord length parametric method, and parametric centroid method are the commonly used methods. Combining the calculation principles of the three calculation methods, the accumulative chord length parametric method is

Table 1
D-H parameters of Dobot magician.

Con-rod i	$\theta_i/^\circ$	$\alpha_{i-1}/^\circ$	a_{i-1}/mm	d_i/mm
1	θ_1	0	0	$d = 103$
2	θ_2	90	0	0
3	θ_3	0	$a_1 = 135$	0
4	θ_4	0	$a_2 = 147$	0

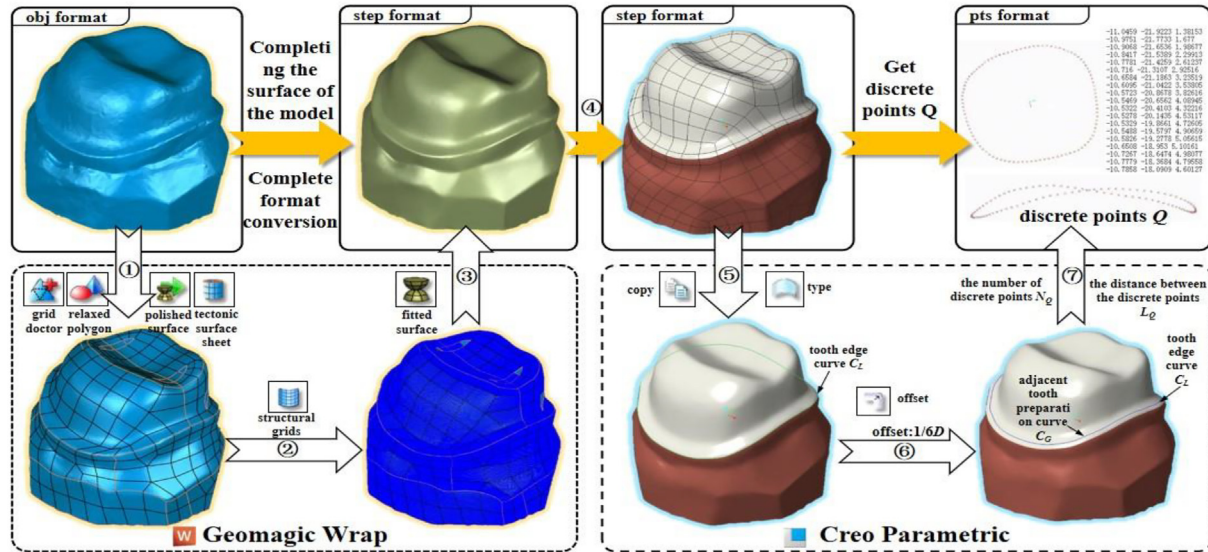
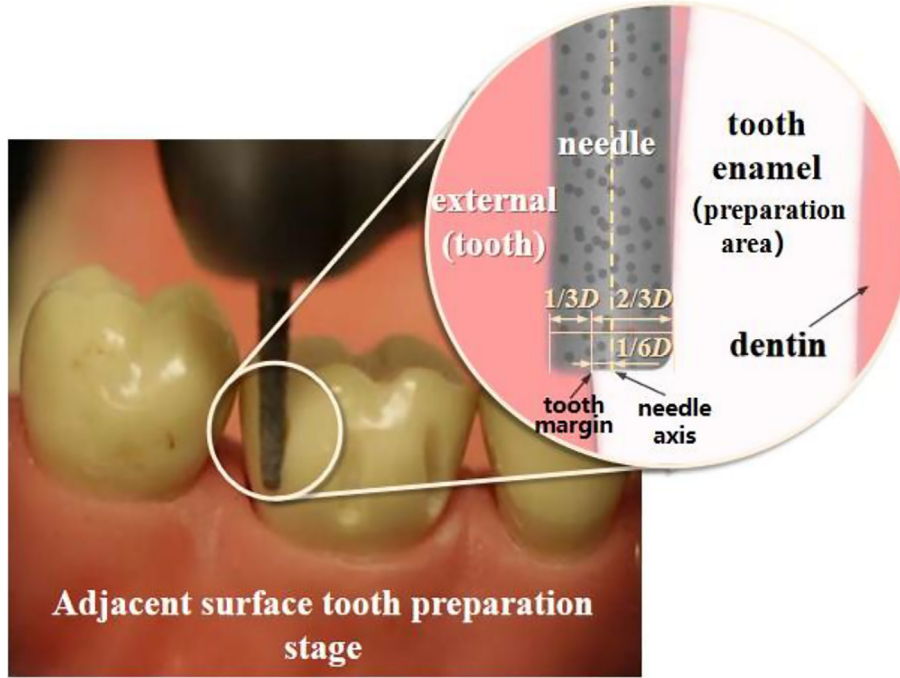


Fig. 7. Preprocessing of standard posterior preparation model.

Fig. 8. Adjacent surface tooth preparation curve C_G extraction criteria.

chosen, which is highly versatile according to the characteristics of the adjacent surface preparation curve. The adjacent surface preparation curve is a closed three-dimensional curve, so the first and last data points of the adjacent surface preparation curve overlap $Q_0 = Q_m$. The adjacent surface preparation curve is 4 degrees of freedom three times the NURBS curve, the first and last three control points are equal in sequence, and the equation is $P_0 = P_{n-2}$, $P_1 = P_{n-1}$, $P_2 = P_n$. NURBS curve mathematical model.

$$C(u) = \sum_{i=0}^n \frac{N_{i,p}(u)\omega_i}{\sum_{j=0}^n N_{j,p}(u)\omega_j} P_i = \frac{\sum_{i=0}^n N_{i,p}(u)\omega_i P_i}{\sum_{i=0}^n N_{i,p}(u)\omega_i} \quad a \leq u \leq b \quad (9)$$

where: ω_i ($i = 0, 1, \dots, n$) is the weighting factor; P_i ($i = 0, 1, \dots, n$) is the control point of the adjacent surface tooth preparation curve,

the number of which is $n + 1$; p is the number of NURBS curves; $N_{i,p}(u)$ is the base function.

$N_{i,p}(u)$ can be defined by the Cox-De Boor recurrence formula.

$$\begin{cases} N_{i,0}(u) = \begin{cases} 1, & u_i \leq u \leq u_{i+1} \\ 0, & \text{else} \end{cases} \\ N_{i,p}(u) = \frac{u - u_i}{u_{i+p} - u_i} N_{i,p-1}(u) + \frac{u_{i+p+1} - u}{u_{i+p+1} - u_{i+1}} N_{i+1,p-1}(u) \end{cases} \quad (10)$$

where u_i is the element of the non-uniform node vector U , as shown in Eq. (11).

$$U = \{u_0, \dots, u_m\} = \left\{ \underbrace{a, \dots, a}_{p+1}, u_{p+1}, \dots, u_{m-p-1}, \underbrace{b, \dots, b}_{p+1} \right\} \quad (11)$$

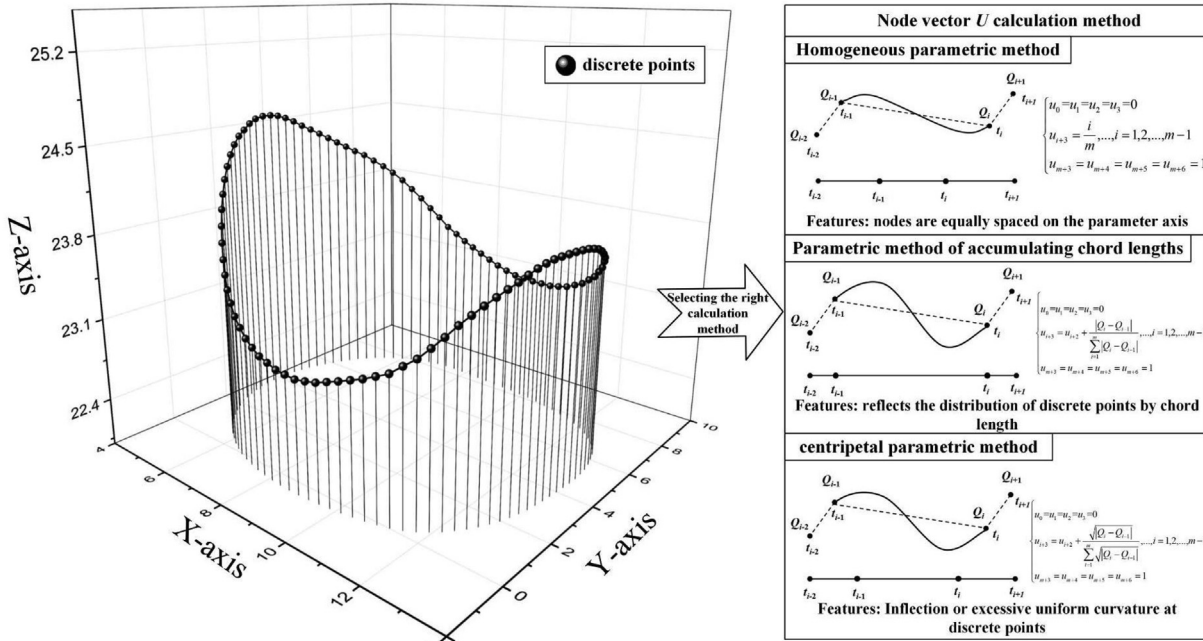


Fig. 9. Discrete points of the adjacent surface tooth preparation curve and three methods for calculating the node vector U .

where $m + 1$ is the length of the node vector U ; m , p , and n are $m = n + p + 1$; and a and b are usually 0 and 1.

In order to facilitate the calculation of the control point P of the adjacent surface tooth preparation curve, the rational division of the NURBS curve is expressed in the form of a matrix.

$$C_i(u) = M_i \begin{bmatrix} \omega_{i-3} P_{i-3} \\ \omega_{i-2} P_{i-2} \\ \omega_{i-1} P_{i-1} \\ \omega_i P_i \end{bmatrix} (1t^2 t^3)/(1t^2 t^3) M_i \begin{bmatrix} \omega_{i-3} \\ \omega_{i-2} \\ \omega_{i-1} \\ \omega_i \end{bmatrix} \quad (i = 3, 4, 5, \dots, n) \quad (12)$$

where $t \in [0, 1]$ M_i is shown in equations (11); order $\Delta_i^k = u_{i+k} - u_i$; special $\Delta_i = u_{i+1} - u_i$.

$$M_i = \begin{bmatrix} m_{11} & m_{12} & m_{13} & m_{14} \\ m_{21} & m_{22} & m_{23} & m_{24} \\ m_{31} & m_{32} & m_{33} & m_{34} \\ m_{41} & m_{42} & m_{43} & m_{44} \end{bmatrix} \quad (13)$$

$$\text{where, } m_{11} = (\Delta_{i+3})^2 / (\Delta_{i+2}^2 \Delta_{i+2}^3), \quad m_{12} = m_{21} = 1 - m_{11} - m_{13}, \\ m_{13} = m_{31} = (\Delta_{i+2})^2 / (\Delta_{i+2}^2 \Delta_{i+2}^3), \\ m_{23} = m_{32} = (3\Delta_{i+2} \Delta_{i+3}) / (\Delta_{i+2}^2 \Delta_{i+2}^3), \quad m_{33} = 3(\Delta_{i+3})^2 / (\Delta_{i+2}^2 \Delta_{i+2}^3), \\ m_{34} = m_{43} = (1/3m_{33} + m_{44} + ((\Delta_{i+3})^2 / (\Delta_{i+3}^2 \Delta_{i+2}^2))) \\ m_{44} = (\Delta_{i+3})^2 / (\Delta_{i+3}^2 \Delta_{i+2}^2)$$

Based on the determined boundary conditions at the beginning and end of the adjacent surface tooth preparation curve, the following formula is used to calculate the control point of the adjacent surface tooth preparation curve in the case of a closed curve.

$$\begin{bmatrix} B_1 & C_1 & A_1 \\ A_2 & B_2 & C_2 \\ \vdots & \ddots & \ddots \\ A_{n-3} & B_{n-3} & C_{n-3} \\ C_{n-2} & A_{n-2} & B_{n-3} \end{bmatrix} \begin{bmatrix} P_1 \\ P_2 \\ \vdots \\ P_{n-3} \\ P_{n-2} \end{bmatrix} = \begin{bmatrix} E_1 \\ E_2 \\ \vdots \\ E_{n-3} \\ E_{n-2} \end{bmatrix} \quad (14)$$

The parameters of the formula are shown in equation (15).

$$\left\{ \begin{array}{l} A_i = (\Delta_{i+2})^2 / \Delta_i + \Delta_{i+1} + \Delta_{i+2} \\ B_i = (\Delta_{i+2}(\Delta_i + \Delta_{i+1}) / \Delta_i + \Delta_{i+1} + \Delta_{i+2}) \\ + (\Delta_{i+1}(\Delta_{i+2} + \Delta_{i+3}) / \Delta_{i+1} + \Delta_{i+2} + \Delta_{i+3}) \\ C_i = (\Delta_{i+1})^2 / \Delta_{i+1} + \Delta_{i+2} + \Delta_{i+3} \\ E_i = (\Delta_{i+1} + \Delta_{i+2}) Q_{i-1} \end{array} \right. \quad (15)$$

where,

Therefore, it is possible to approximate the original adjacent surface tooth preparation curve by using the discrete points Q of the adjacent surface tooth preparation curve, the node vector U of the adjacent surface tooth preparation curve, the control point P of the adjacent surface tooth preparation curve, and the set weighting factor ω .

2.3.2. Interpolation of tooth preparation curves on adjacent surfaces

In order to make the robot complete the expected adjacent surface tooth preparation curve accurately, the curve needs to be divided theoretically. The more segments that are divided, the closer the robot's end trajectory will be to the expected curve. Therefore, based on the inverse calculation of the adjacent surface preparation curve based on NURBS curve interpolation to complete the robot's trajectory planning of adjacent surface preparation curve. The interpolation principle of NURBS is to use the time series $\{t_1, t_2, \dots, t_k, \dots, t_{n-1}, t_n\}$ to segment the parameter sequence $\{u_1, u_2, \dots, u_k, \dots, u_{n-1}, u_n\}$, and then get the interpolation point sequence $\{C(u_1), C(u_2), \dots, C(u_k), \dots, C(u_{n-1}), C(u_n)\}$, the core calculation of interpolation is to find the relationship between u_k and u_{k+1} by using the interpolation period T , and further get $C(u_{k+1})$ by $C(u_k)$. The derivation of equation (9) yields.

$$\frac{dC(u)}{du} = C^{(1)}(u) = \frac{\sum_{i=0}^n N_{i,p}(u) \omega_i P_i}{\sum_{i=0}^n N_{i,p}(u) \omega_i^2} = \frac{\sum_{i=0}^n N_{i,p}(u) \omega_i P_i}{\left[\sum_{i=0}^n N_{i,p}(u) \omega_i \right]^2} \quad (16)$$

where, $C^{(1)}(u)$ is the first-order derivative of the curve pair u .

Continuing with the second derivative of the adjacent surface tooth preparation curve, we get:

$$\begin{aligned} \frac{d^2C(u)}{du^2} &= C^{(2)}(u) \\ &= \frac{N_{i,p}^{(2)}(u)\omega_i P_i}{\sum_{i=0}^n N_{i,p}(u)\omega_i} + \frac{2N_{i,p}(u)\omega_i P_i \left[\sum_{i=0}^n N_{i,p}^{(1)}(u)\omega_i \right]^2}{\left[\sum_{i=0}^n N_{i,p}(u)\omega_i \right]^3} - \\ &\quad \frac{2N_{i,p}(u)\omega_i P_i \sum_{i=0}^n N_{i,p}^{(1)}(u)\omega_i + \omega_i N_{i,p}(u)P_i \sum_{i=0}^n N_{i,p}^{(2)}(u)\omega_i}{\left[\sum_{i=0}^n N_{i,p}(u)\omega_i \right]^2} \end{aligned} \quad (17)$$

where $C^{(2)}(u)$ is the second-order derivative of the adjacent surface prepared tooth curve for u . The expression for the base function $N_{i,p}^{(m)}(u)$ is:

$$N_{i,p}^{(m)}(u) = p \left[\frac{N_{i,p-1}^{(m-1)}(u)}{u_{i+p} - u_i} - \frac{N_{i+1,p-1}^{(m-1)}(u)}{u_{i+p+1} - u_{i+1}} \right] \quad (18)$$

The feed rate on the NURBS curve is expressed as:

$$V(t) = \frac{dC(u)}{dt} = \frac{dC(u)}{du} \cdot \frac{du}{dt} \quad (19)$$

Rectifying the transformation formula (17) yields.

$$\frac{du}{dt} = \frac{V(t)}{\frac{dC(u)}{dt}} = \frac{V(t)}{\sqrt{C_x^{(1)}(u_k)^2 + C_y^{(1)}(u_k)^2 + C_z^{(1)}(u_k)^2}} \quad (20)$$

where $C_x^{(1)}(u_k)$ is the first-order derivative in the x-direction of the curve, $C_y^{(1)}(u_k)$ is the first-order derivative in the y-direction of the curve, and $C_z^{(1)}(u_k)$ is the first-order derivative in the z-direction of the curve.

Continuing with the second-order derivative of Eq. (20), we can obtain:

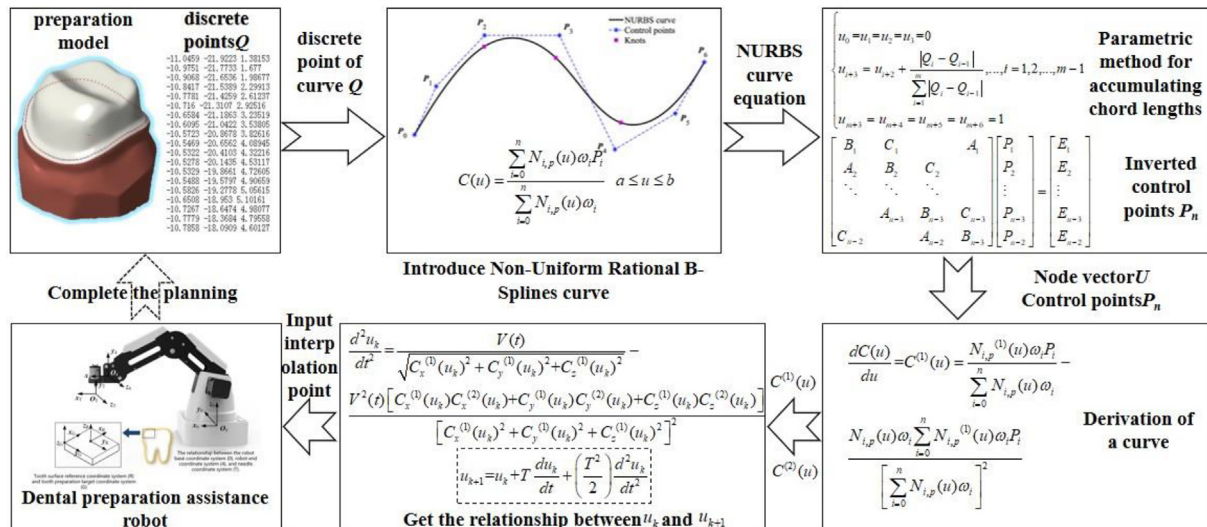


Fig. 10. Robot trajectory planning process for the adjacent surface tooth preparation curve.

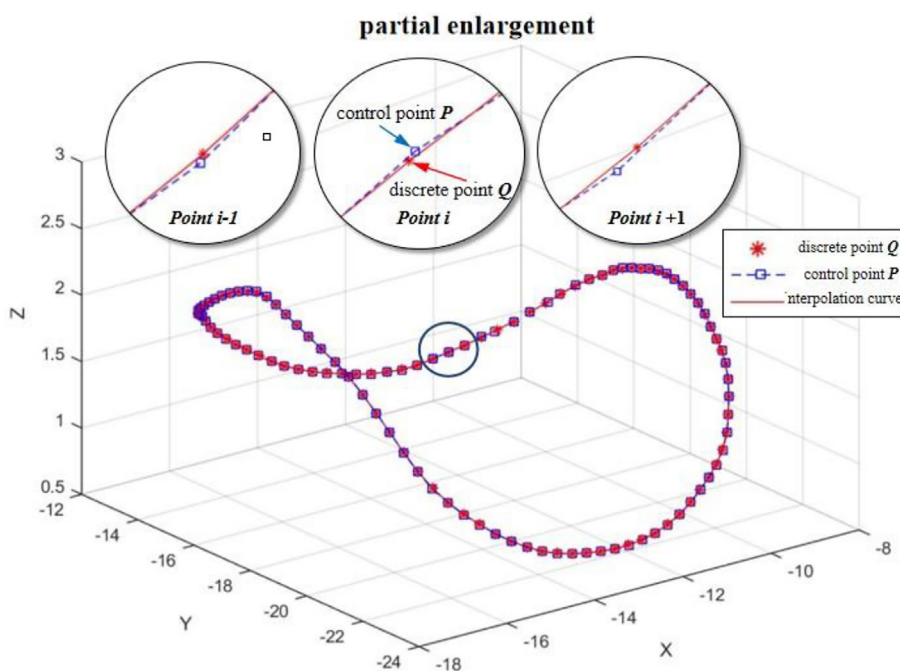


Fig. 11. Interpolation result of adjacent surface tooth preparation curve.

$$\frac{d^2u_k}{dt^2} = \frac{V(t)}{\sqrt{C_x^{(1)}(u_k)^2 + C_y^{(1)}(u_k)^2 + C_z^{(1)}(u_k)^2}} - \\ V^2(t)[C_x^{(1)}(u_k)C_x^{(2)}(u_k) + C_y^{(1)}(u_k)C_y^{(2)}(u_k) + C_z^{(1)}(u_k)C_z^{(2)}(u_k)] \\ [C_x^{(1)}(u_k)^2 + C_y^{(1)}(u_k)^2 + C_z^{(1)}(u_k)^2]^2 \quad (21)$$

where $C_x^{(2)}(u_k)$ is the second-order derivative in the x-direction of the curve, $C_y^{(2)}(u_k)$ is the second-order derivative in the y-direction of the curve, and $C_z^{(2)}(u_k)$ is the second-order derivative in the z-direction of the curve.



Fig. 12. Packages loading and XR option.

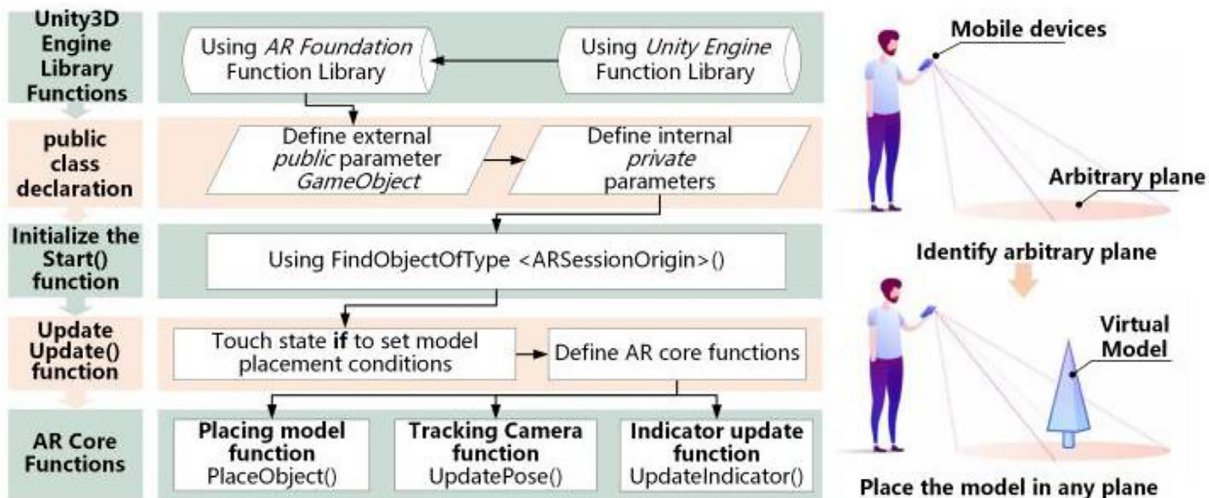


Fig. 13. Basic process of development and expected result.

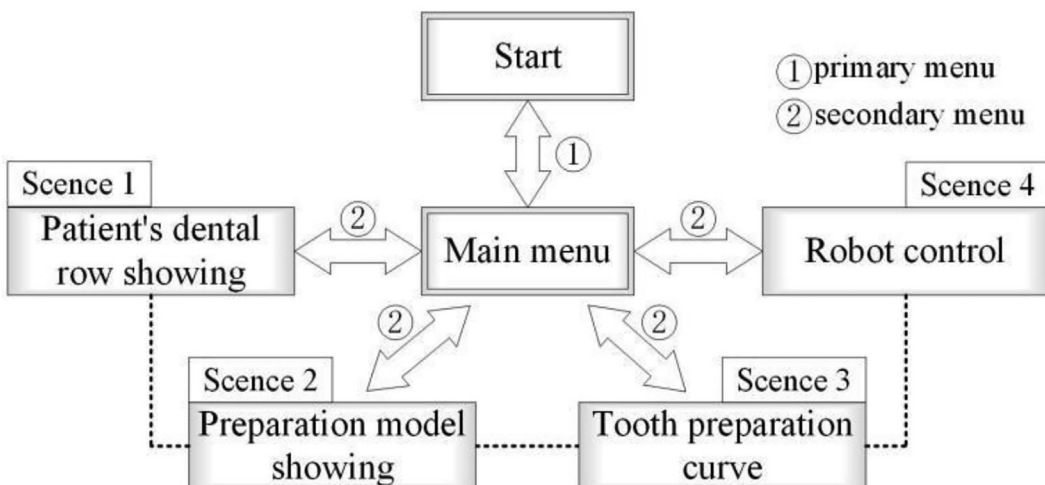


Fig. 14. Relationship between scenes.

In this paper, the relationship between the geometric and kinematic properties of the NURBS curve, i.e., between u_k and u_{k+1} , is obtained by using a second-order Taylor expansion formula.

$$u_{k+1} = u_k + T \frac{du_k}{dt} + \left(\frac{T^2}{2} \right) \frac{d^2 u_k}{dt^2} \quad (22)$$

In summary, the robot trajectory planning process for the adjacent surface tooth preparation curve is shown in Fig. 10.

Through MATLAB software programming, the dental drill diameter D is selected as 1.6 mm, and the curve offset is selected as

0.265, the number of discrete points N_Q take 100, discrete point increment L_Q take 0.01, interpolation period $T = 0.002$ s, the interpolation results shown in Fig. 11.

2.4. Augmented reality-based dental preparation assistance software

While introducing robots to assist doctors in the preparation of teeth, the human-robot interaction is an important part of the process that determines whether the doctor can easily and quickly control the robot. In addition, the tooth structure is small and the preparation process requires a high degree of precision, which

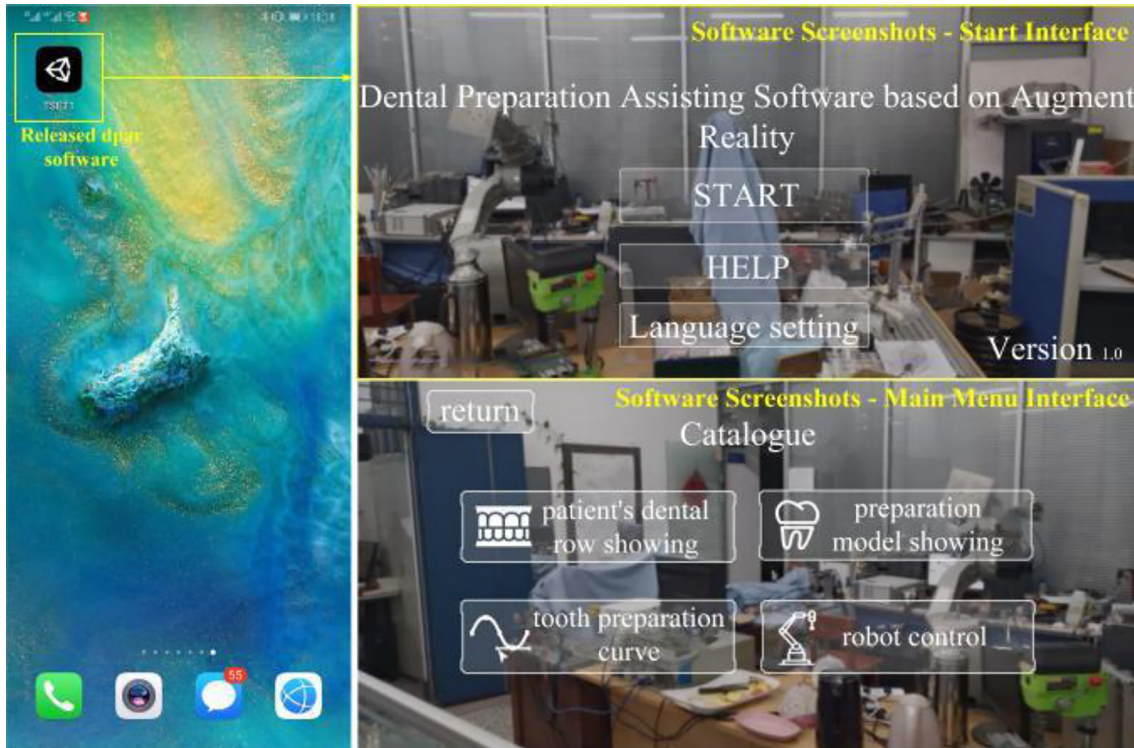


Fig. 15. Published DPAS AR and software screenshots.

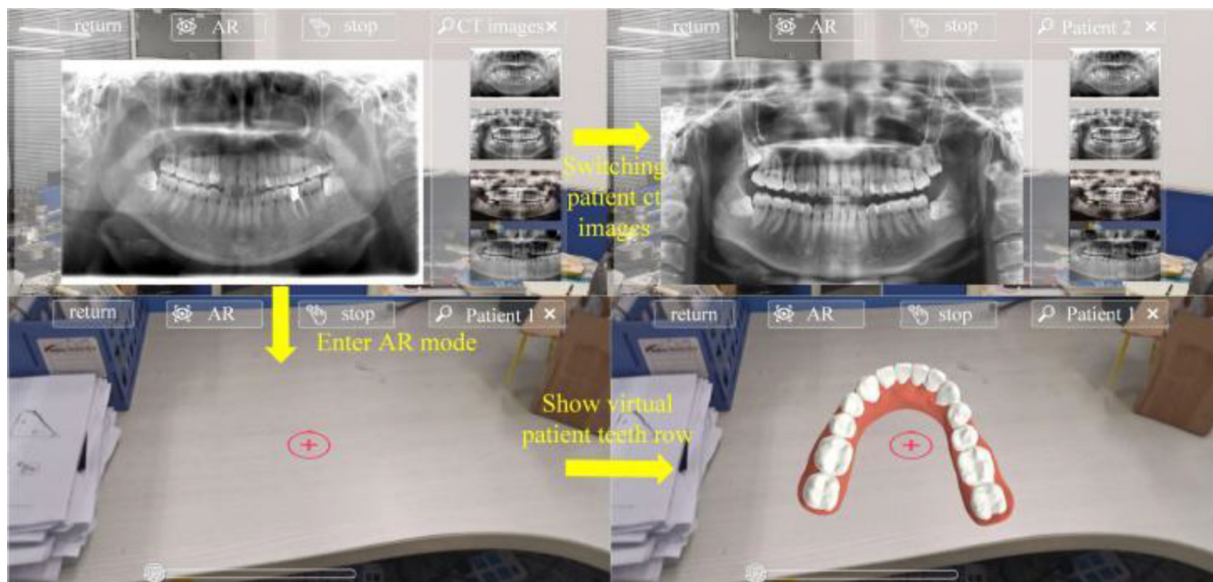


Fig. 16. Display patient dentition.

cannot be visualized by the traditional display method of viewing the patient's tooth model and standardizing the preparation information and the preparation plan. Therefore the assisted software of tooth preparation based on augmented reality is developed by

improving human-computer interaction through a virtual-reality environment. In this paper, the augmented reality based on AR Foundation is developed by selecting one of the ARCore SDK as the specific development tool, and the software runs on Android



Fig. 17. Preparation model and 3D curved planning.



Fig. 18. Robot control scene.

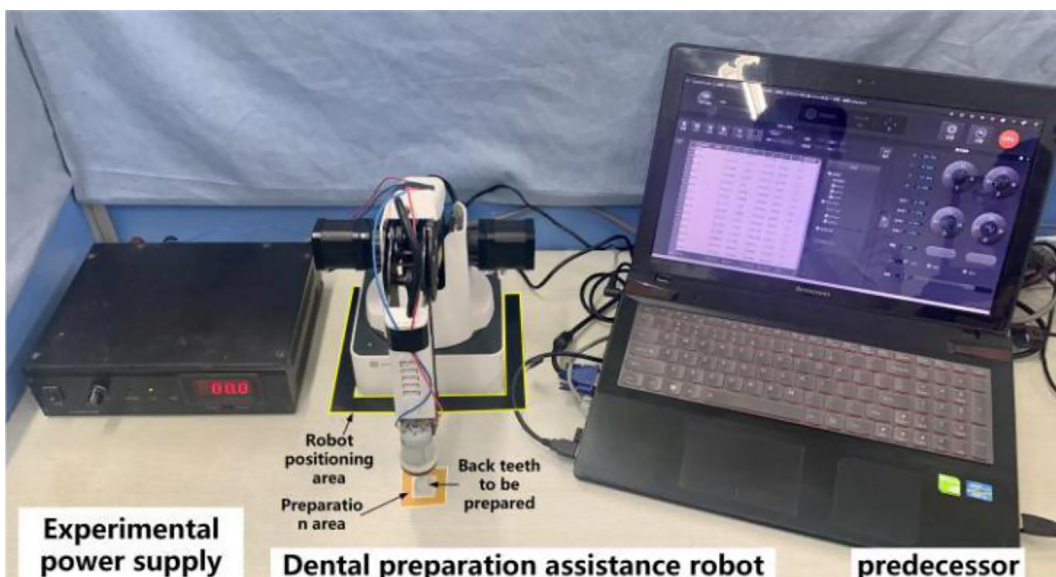


Fig. 19. Experiment system of robot-assisted tooth preparation.

system. Before writing the C# program, we load the packages in Unity 3D, and load the *AR Foundation*, *ARCore XR Plugin* and *ARKit XR Plugin* packages. "The options include "AR Session Origin", "AR Session", "AR Default Point Cloud" and other options for subsequent calls, Packages are loaded with XR options as shown in Fig. 12.

The software development process based on *AR Foundation* augmented reality is mainly divided into calling Unity3D library functions, defining external parameters and internal parameters, initializing *Strat()* function, updating *Update()* function and *AR core function*. Among them, except for the AR core function, the rest of the steps are the basic process of Unity3D development process,

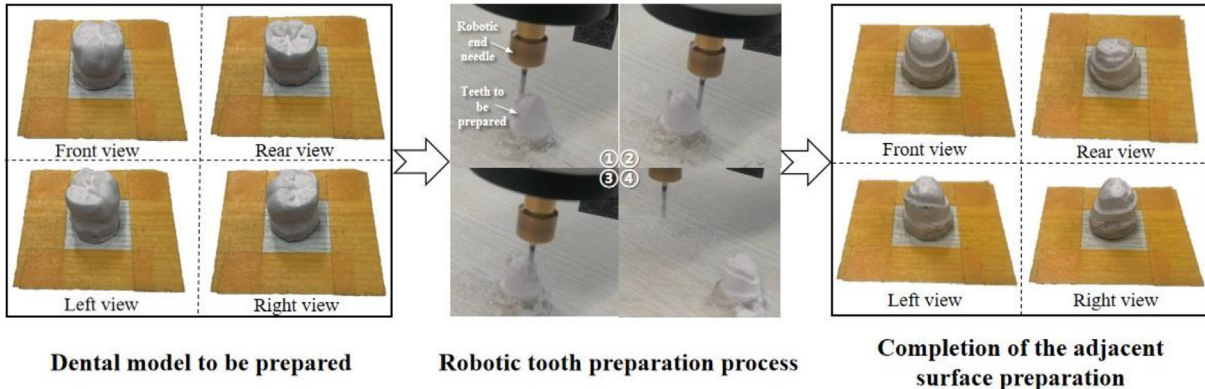


Fig. 20. Experiment process of robot completing the adjacent surface preparation phase.

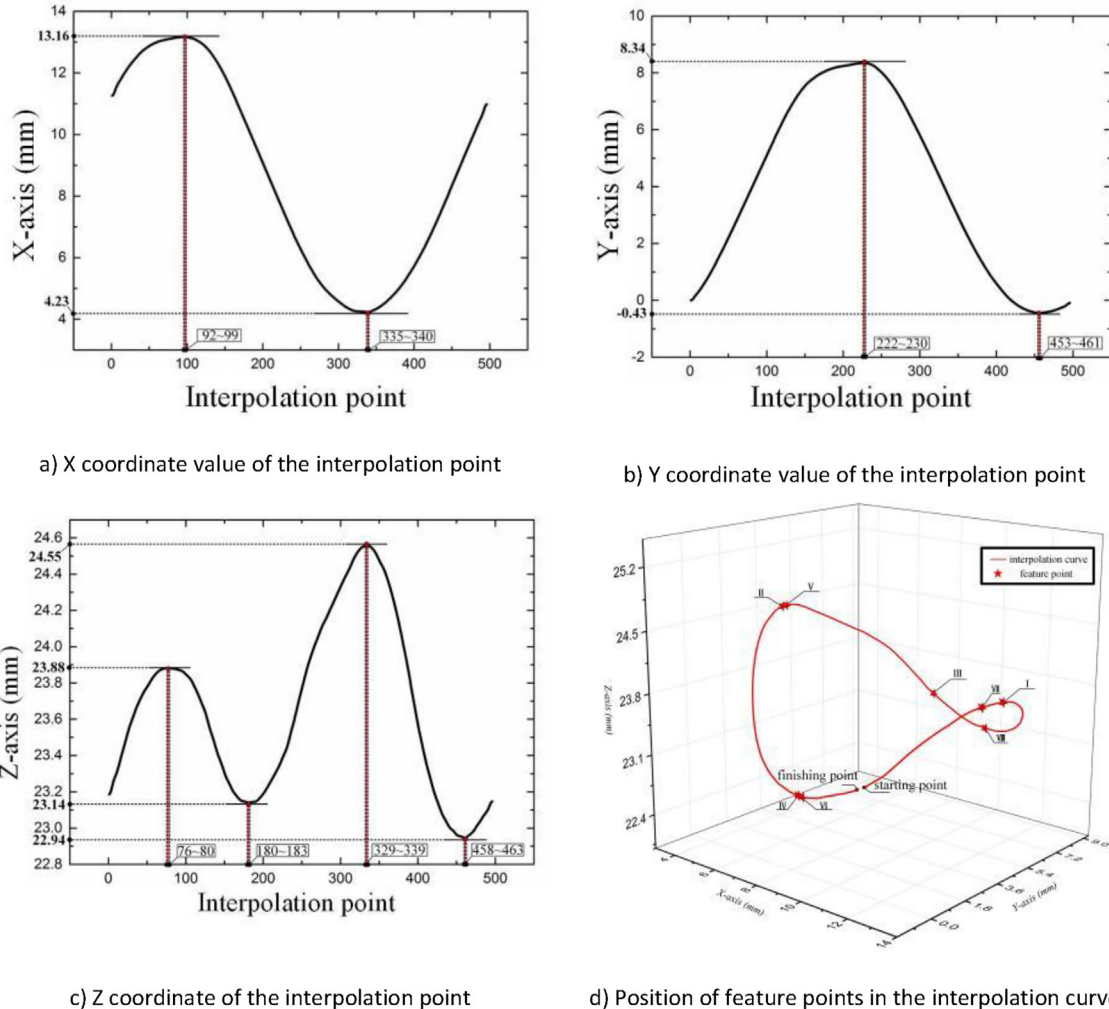


Fig. 21. Selection of feature points in adjacent surface preparation.

the programming language of the development process is C#, and the compiler is Microsoft Visual Studio 2019. The basic process of development is shown in the Fig. 13.

The start interface, main menu, and four functional scenes of the UI design are mainly completed in the software. The software name, version number, and other information are included in the start interface. The main menu is used to guide the four functional scenes, which are 'patient's dental row showing', 'preparation model showing', 'tooth preparation curve', and 'robot control'. The relationship between the various scenes is shown in Fig. 14. Mobile-exclusive touch interaction is chosen as augmented reality

interactions, and the mobile device is Huawei Mate 20 Pro, 1920*1080 widescreen of the "Game" option in Unity3D is selected. The images collected by the mobile camera in real-time are used as the dynamic background of each interface in software, for achieving a better combination between reality and virtual reality. The Android platform has 6 GB RAM and operating system, and the published DPAS AR is shown in Fig. 15.

2.4.1. Display of a patient's tooth

In the main menu, select "patient's teeth showing" to enter the scene one, and you can select and view the patient's dental CT

Table 2

The theoretical value of feature points during the adjacent surface preparation phase.

feature point coordinate	Interpolation point X-direction		Interpolation point Y-direction		Interpolation point Z-direction			
	I	II	III	IV	V	VI	VII	VIII
x/mm	13.16	4.24	7.58	8.74	4.24	8.95	13.10	10.16
y/mm	4.83	3.66	8.35	-0.43	3.87	-0.43	3.72	8.12
z/mm	23.86	24.55	23.40	22.95	24.56	22.95	23.88	23.14

Table 3

The experimental measurement value of feature points.

Number of measurements	Feature point	1	2	3	4	5
I		(13.27, 4.66, 24.11)	(12.95, 4.77, 23.66)	(13.21, 4.60, 23.68)	(13.35, 4.92, 23.44)	(13.22, 4.50, 24.01)
II		(4.07, 3.72, 24.38)	(4.51, 4.03, 24.70)	(4.19, 3.88, 24.22)	(4.33, 3.95, 24.80)	(4.42, 4.20, 24.89)
III		(7.52, 8.01, 23.37)	(7.11, 8.57, 23.61)	(7.26, 8.17, 23.08)	(7.94, 8.49, 23.24)	(7.15, 8.25, 23.08)
IV		(8.66, -0.44, 23.25)	(8.47, -0.40, 22.71)	(8.56, -0.45, 22.60)	(9.20, -0.43, 23.20)	(8.67, -0.38, 22.80)
VII		(13.14, 2.92, 23.33)	(12.91, 3.93, 23.54)	(13.19, 3.57, 24.02)	(13.26, 3.79, 24.18)	(13.41, 3.60, 23.98)
VIII		(10.42, 8.32, 23.62)	(9.80, 8.17, 23.48)	(10.34, 7.95, 23.73)	(10.58, 7.87, 23.66)	(10.09, 8.23, 23.06)

Table 4

Statistical table of various parameters of system error.

Direction	Parameter	Feature point					
		I	II	III	IV	VII	VIII
X-direction	μ/mm	13.19	4.30	7.39	8.70	13.18	10.24
	ε/mm	0.03	0.06	0.18	0.24	0.08	0.09
	RSD/%	1.12	4.14	4.64	3.26	1.38	2.98
	confidence interval	[13.09, 13.28]	[4.19, 4.41]	[7.18, 7.62]	[8.54, 8.90]	[13.05, 13.29]	[10.03, 10.43]
Y-direction	μ/mm	4.68	3.95	8.29	-0.42	3.56	8.10
	ε/mm	0.14	0.29	0.05	0.02	0.15	0.02
	RSD/%	3.42	4.49	2.77	6.84	10.82	2.35
	confidence interval	[4.58, 4.80]	[3.84, 4.06]	[8.15, 8.44]	[-0.44, -0.40]	[3.29, 3.77]	[7.98, 8.22]
Z-direction	μ/mm	23.77	24.59	23.28	22.91	23.80	23.51
	ε/mm	0.08	0.04	0.11	0.03	0.07	0.37
	RSD/%	1.15	1.15	0.59	1.28	1.51	1.14
	confidence interval	[23.60, 23.95]	[24.38, 24.76]	[23.14, 23.43]	[22.70, 23.12]	[23.55, 24.04]	[23.31, 23.66]

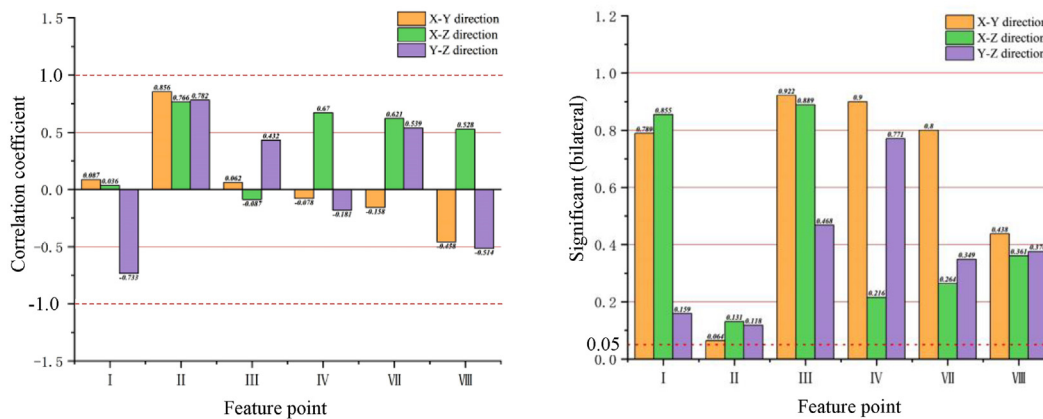


Fig. 22. Statistical figure of random error correlation coefficients.

images through the patient CT images on the right side, and switch between CT images according to the doctor's or user's needs. After selecting a patient's CT image, click on the preset "AR mode" to enter AR mode and double click on the screen to complete the placement of the model. The scene showing the patient's tooth rows is in Fig. 16.

2.4.2. Preparation models and tooth preparation curves

In scene 2 and 3, the preparation model and standardized tooth preparation parameters can be viewed by a physician, as well as three different 2D views of the 3D curve. The doctors can preview the planned robot-assisted adjacent surface preparation trajectory and preparation model in augmented reality using their mobile phones. It also can zoom, rotate, and change the transparency to see the planning information and preview the planning results. The scene of model and curve is shown in Fig. 17.

2.4.3. Robot control

This scene is designed from a robot control perspective, and has the function of AR mode. The communication between the augmented reality software and the robot is realized via Bluetooth. Communication method is GATT (Generic Attribute Profile) protocol. Tooth preparation information and information about the preparation phase of the robot is also shown in the scene. The DPAS AR software controls robot to zero and stop, and the robot will follow the planned trajectory for tooth preparation. The robot control is shown in Fig. 18.

3. Results

3.1. Experimental systems

The experimental system based on the Dobot Magician robotic arm is shown in Fig. 19. The experimental system consists of the experimental power supply, the physical prototype of the tooth preparation assisted robot and the computer.

3.2. Experimental process

During the experiment, the dental drill diameter is 1.6 mm, the experimental voltage is 12 V, the current is 0.25A, the end rotational speed is about 46000r/min, and the robot moves at a speed of 11.1 mm/s for 15% of the set deposit point to playback speed. The robot completes the adjacent surface preparation phase of the experimental process, as shown in Fig. 20.

3.3. Analysis of experimental data

The feature points in the preparation phase of the adjacent surface are obtained by analyzing the known interpolation points. First, the relationship between the three coordinate values of X, Y, and Z and the interpolation points are plotted as a), b), and c) of Fig. 21, respectively. The three curves have different numbers of inflection points, and the inflection points of the three curves are selected as feature points to verify the preparation accuracy of the robot at this stage. When the feature points are selected, there will be multiple interpolation points corresponding to the inflection points. For example, the coordinate value in the X-direction of 13.16 mm corresponds to the 92nd to 99th interpolation points. The accuracy is set to 0.01 mm based on the actual accuracy of the robot. So, it is necessary to obtain the feature point by finding the points corresponding to the value and calculating the mean value. The obtained feature points are shown in Table 2. The position of the feature points and start/finish point in the interpolation curve are shown in Fig. 21 d). It can be seen that each

feature point is at the position where the curve trend changes. And, it is indicated that these feature points are key nodes in the entire process of tooth preparation, which determine the accuracy of the trajectory. Therefore, the feature points are used to verify the accuracy of the robot's adjacent surface preparation. The determination of the start and end points defines the direction of execution of the robotic tooth preparation operation and ensures the integrity of the tooth preparation trajectory planning.

The tooth preparation curve of the adjacent surface completed by the robot was marked and measured based on the position of the feature points in the interpolation curve. During the measurement process, it needs to ensure that the relative positions between teeth and robot are the same to those in the preparation phase. The feature points were measured using the robot's teach mode, and each feature point was measured five times, and the average of the five measurements of the feature point coordinates was recorded as the actual measured value of the feature point. However, according to Table 2 and Fig. 19 d), and in conjunction with the actual measurement process, two sets of feature points (II and V, IV and VI) are very close to each other. It results in similar data for multiple measurements, so, a total of 6 feature points are obtained by reducing the two features (V and VI), as shown in Table 3.

4. Discussion

Due to the influence of multiple factors, the experimental data deviated from the theoretical data, so the corresponding error analysis was performed. Error analysis is performed on the data obtained from the measurements. The errors that exist between the theoretical feature points and the experimental measurements include systematic and random errors. The systematic error consists of several error factors with deterministic variation patterns [23]. In this work, the mean of the measurements μ , the standard deviation s of the measurement sample, and the confidence interval $[\bar{x} - k_1 s, \bar{x} + k_1 s]$ of the mean μ are used to define the boundaries of the systematic error, where \bar{x} is the unbiased estimate of μ and the safety factor k_1 is determined by the percentage of the confidence interval. Relative fixed-point error ε and relative standard deviation RSD are used to evaluate the relative error metrics in the three directions of XYZ [24,25]. Taking the x-axis coordinate value of feature point I as an example, the relative fixed-point error ε_{I-x} is the error of the measurement mean relative to the feature point, standard deviation RSD_{I-x} can be used to check the precision of measurement results, and its expression is shown in Equation 21.

$$\varepsilon_{I-x} = \left| \bar{x}_I - x_I \right| \quad (21)$$

$$RSD_{I-x} = \frac{s_{I-x}}{\bar{x}_I} \times 100\%$$

where $\bar{x}_I = \sum_{i=1}^n x_{I-i} / n$ is the x-axis measurement coordinate value of feature point I; x_I is the theoretical x-axis coordinate value of feature point I in Table 2. s_{I-x} is the standard deviation of the measurement sample of feature point I.

Take the 90% confidence interval, determine the value of k_1 as 0.5796, and then calculate the measurement mean μ , relative fixed-point error ε , relative standard deviation RSD , and confidence interval of the experimental data as shown in Table 4.

As shown in Table 4, the relative fixation errors ε of each feature point in the X, Y and Z directions are 0.03 ~ 0.24, 0.02 ~ 0.29 and 0.03 ~ 0.37 mm, respectively. And, all feature errors can be controlled within 0.5 mm, it ensures that the robot can reach each key node accurately to complete the preparation stage. The relative standard errors (RSD) of each feature point in the X, Y and Z directions range from 1.12 to 4.64%, 2.35 to 10.82% and 0.59 to 1.51%,

respectively. And, it can be found that the RSD of each feature point in the three directions remain stable at less than 11%. Among them, the Z direction has the smallest relative standard error among the three directions, due to the relatively small coordinate change in the Z direction of the adjacent surface preparation phase. The relative standard errors in the X and Y directions for the remaining two directions have a large coordinate variation, which is caused by the large influence of the measurement accuracy and coordinate system transformation matrix. The widths range of the confidence intervals of each feature point in the X, Y, and Z directions is 0.18 to 0.43, 0.03 to 0.48, and 0.29 to 0.49 mm, respectively. The average width of the confidence interval in different directions under the same feature point is stable at about 0.31 mm. It indicates that the systematic error can be stabilized in a small range at each feature point in the adjacent surface tooth preparation stage, and the preparation accuracy of the robot can be ensured.

In this paper, the significance test and Pearson's correlation coefficient are used to evaluate the random correlation in each direction, where the value of the significance test is used to determine whether the two are correlated. And, the Pearson's correlation coefficient is used to determine the degree of correlation. Three sets of random two-dimensional variables are set up according to the measured data in total, which are random error in X and Y directions, random error in X and Z directions, and random error in Y and Z directions, respectively. The random error correlation coefficients are shown in Fig. 22.

The characteristic values of each feature point in the X and Y, X and Z, Y and Z directions is range from 0.064 to 0.922, 0.131 to 0.889, and 0.118 to 0.771, respectively. The values of significance tests were all greater than 0.05, so it can be found that there is no linear relationship between the two directions of each feature point. The numerical range of the correlation coefficients of each feature point in the X and Y, X and Z, Y and Z directions are $-0.458\text{--}0.856$, $-0.087\text{--}0.766$ and $-0.733\text{--}0.782$, respectively. The absolute values of each correlation coefficient are not close to 1, so it can be shown that the correlation between the feature points in the three directional variables is not strong. The feasibility and correctness of the robotic trajectory planning method of adjacent surface tooth preparation and the use of robots for tooth preparation were verified.

5. Conclusion

In this paper, we establish a robotic adjacent tooth preparation trajectory planning algorithm based on the characteristics of adjacent tooth preparation to automate the preparation of adjacent teeth. An augmented reality-based dental preparation aid app is designed using Unity3D to provide a virtual-reality environment for the surgeon to visualize the preparation process and improve human-robot interaction through computer simulation. Finally, a robotic tooth-adjacent surface preparation experiment was performed, the relative fixation errors of the feature points in the X, Y and Z directions are 0.03–0.24, 0.02–0.29 and 0.03–0.37 mm, respectively, and the error of all feature points does not exceed 0.5 mm. The relative standard errors in the X, Y and Z directions were 1.12–4.64%, 2.35–10.82% and 0.59–1.51%, respectively, and the relative standard errors in the X, Y and Z directions remained stable and were all less than 11%. The results show that the augmented reality-based tooth preparation-assisted robot can achieve full crown adjacent surface preparation of posterior teeth within the margin of error.

Declaration of Competing Interest

The authors declare that they have no known competing financial interests or personal relationships that could have appeared to influence the work reported in this paper.

Acknowledgments

This research was supported by China Postdoctoral Science Foundation Special Funded Project (Grant No. 2018T110313), and Fundamental Research Foundation for Universities of Heilongjiang Province (Grant No. LGYC2018JQ016).

References

- [1] P. Phantumvanit, Y. Makino, H. Ogawa, A. Rugg-Gunn, C. Ungchusak, WHO Global Consultation on Public Health Intervention against Early Childhood Caries, *Commun. Dent. Oral.* 46 (3) (2018) 280–287.
- [2] S. Liang, F. Yuan, High-accuracy digital model design for full crown tooth preparation, *Int. J. Comput. Dent.* 22 (4) (2019) 331–342.
- [3] B. Zhang, N. Dai, S. Tian, F. Yuan, Q. Yu, The extraction method of tooth preparation margin line based on S-Octree CNN, *Int. J. Numer. Meth. Bio.* 35 (10) (2019), <https://doi.org/10.1002/cnm.v35.1010.1002/cnm.3241>.
- [4] F.S. Yuan, J.Q. Zheng, Y.P. Zhang, Y. Wang, Y.C. Sun, P.J. Lyu, Preliminary study on the automatic preparation of dental implant socket controlled by micro-robot, *Chin. J. Stomatol.* 53 (8) (2018) 524–528.
- [5] M.Q. Zhou, J.N. Zhang, J. Hong, Application of robots in stomatology, *Shanghai J. Stomatol.* 25 (5) (2016) 626–629.
- [6] J.L.O. Simon, A.M. Martinez, D.L. Espinoza, J.G.R. Velazquez, Mechatronic assistant system for dental drill handling, *Int. J. Med. Robotics Comput. Assist. Surg.* 7 (2011) 22–26.
- [7] H. Feng, L. Wang, L.J. Xing, T.T. Jia, Y.B. Chen, R. Zhao, H.Z. Zhang, Design of a robot system for oral and dental Treatment, *China Med. Devic.* 32 (04) (2017) 30–32.
- [8] T. Otani, A.J. Raigrodski, L. Mancl, I. Kanuma, J. Rosen, In vitro evaluation of accuracy and precision of automated robotic tooth preparation system for porcelain laminate veneers, *J. Prosthet. Dent.* 114 (2) (2015) 229–235.
- [9] Bello, N. A study of the accuracy of a prototype computer numerical control dental hand-piece compared to manual preparation for a full coverage crown preparation. 2016.
- [10] J. Grischke, L. Johannsmeier, L. Eich, L. Griga, S. Haddadin, Dentronics: Towards robotics and artificial intelligence in dentistry, *Dent. Mater.* 36 (6) (2020) 765–778.
- [11] N. Dai, Y. Zhong, H. Liu, F.S. Yuan, Y. Sun, Digital modeling technology for full dental crown tooth preparation, *Comput. Biol. Med.* 71 (1) (2016) 190–197.
- [12] F.S. Yuan, Y. Wang, Y.P. Zhang, Y.C. Sun, P.J. Lyu, Study on the appropriate parameters of automatic full crown tooth preparation for dental tooth preparation robot, *Chin. J. Stomatol.* 52 (5) (2017) 270–273.
- [13] F. Yuan, P. Lyu, A preliminary study on a tooth preparation robot, *Adv Appl Ceram.* 119 (5–6) (2020) 332–337.
- [14] F. Yuan, Y. Wang, Y. Zhang, Y.C. Sun, D.X. Wang, P.J. Lyu, An automatic tooth preparation technique: A preliminary study, *Sci. Rep.-UK* 6 (2016) 1–9.
- [15] D.X. Wang, L. Wang, Y.R. Zhang, P.J. Lv, Y.C. Sun, J. Xiao, Preliminary study on a miniature laser manipulation robotic device for tooth crown preparation, *Int. J. Med. Robot. Comp.* 10 (4) (2015) 482–494.
- [16] L. Wang, D.X. Wang, Y.R. Zhang, L. Ma, Y.C. Sun, P.J. Lv, An automatic robotic system for three-dimensional tooth crown preparation using a picosecond laser, *Laser Surg. Med.* 46 (7) (2014) 7573–7581.
- [17] A.E. Solyman, M. Roman, H.I. Saleh, M. Atia, K.M. Ibrahim, Perceptive augmented reality-based interface for robot task planning and visualization, *Int J Innov Comput I.* 16 (5) (2020) 1769–1785.
- [18] N.G. Timmons, B. Huang, Q. Li, in: *Augmented Reality with Multi-view Merging for Robot Teleoperation*, Association for Computing Machinery, New York, USA, 2020, pp. 260–262.
- [19] F.X. Zhang, C.Y. Lai, M. Simic, S.L. Ding, Augmented reality in robot programming, *Proc. Computer Sci.* 176 (2020) 1221–1230.
- [20] J.D. Hernandez, S. Sobti, A. Sciola, M. Moll, L.E. Kavraki, Increasing robot autonomy via motion planning and an augmented reality interface, *IEEE Robot Autom. Let.* 5 (2) (2020) 1017–1023.
- [21] Chacko, S. M.; Kapila, V. Augmented Reality as a Medium for Human-Robot Collaborative Tasks in 2019 28th IEEE International Conference on Robot and Human Interactive Communication (RO-MAN). New Delhi, India, 2019, 1–8.
- [22] A. Abbasnia, C. Guedes Soares, Exact evaluation of hydrodynamic loads on ships using NURBS surfaces and acceleration potential, *Eng. Anal. Bound. Elem.* 85 (2017) 1–12.
- [23] J.P. Sun, X. Jeff, Z.P. Tang, Study on robot accuracy compensation method based on approximation degree weighted average interpolation, *Chin. J. Sci. Instrum.* 40 (11) (2019) 128–173.
- [24] J. Jiang, Z. Huang, W. Qian, Y. Zhang, Y. Liu, Registration technology of augmented reality in oral medicine: A review, *IEEE Access.* 7 (2019) 53566–53584.
- [25] J.G. Jiang, Z.Y. Huang, X.W. Guo, Y.D. Zhang, Y. Xu, Study on the design and experiment of RCM of transrectal ultrasound probe posture adjustment, *Chin. J. Sci. Instrum.* 40 (2) (2019) 164–173.